Journal of Integral Sciences
[An International Open Access Journal]
Available at www.jisciences.com ISSN: 2581-5679

SYNTHESIS, SPECTROSCOPIC CHARACTERIZATION, AND COMBINED DFT/GFN2-XTB STUDY OF ETHYL 4-[2-(3-HYDROXY-4-METHOXYPHENYL)-4,9-DIOXO-2,3,4,9-TETRAHYDRO-1,3-BENZOXAZEPIN-3-YL] BENZOATE

RAWAA NAEAMAH ABDULLAH

Ministry of Education, General Directorate of Al-Qadisiyah Education, Diwaniyah, Iraq

Received: 04-05-2026 Revised: 24-05-2026 Accepted: 16-08-2026

ABSTRACT

A new seven-membered oxygen/nitrogen heterocycle, ethyl 4-[2-(3-hydroxy-4-methoxyphenyl)-4,9-dioxo-2,3,4,9-tetrahydro-1,3-benzoxazepin-3-yl]benzoate (2), was synthesized in two steps from isovanillin and benzocaine. Acid-catalyzed condensation produced azomethine 1, followed by [2+5] cycloaddition with phthalic anhydride to form the seven-membered ring without loss of a small molecule. Both compounds were characterized by FT-IR and $^{1}H/^{13}C$ NMR spectroscopy. Formation of 2 was confirmed by disappearance of the azomethine band at 1642 cm^{-1} and appearance of lactone and lactam carbonyl bands at 1709 and 1674 cm^{-1}, respectively. The phenolic O–H bands shifted from 3369 cm^{-1} in 1 to 3213 and 3113 cm^{-1} in 2, indicating stronger hydrogen bonding. The azomethine carbon resonance at 162.1 ppm was replaced by lactam and lactone carbonyl signals at 174.9 and 169.2 ppm. Computational studies using B3LYP/6-31G(d), supported by ETKDG, MMFF94, and GFN2-xTB conformational analysis, showed that the heterocycle adopts a twist-boat conformation with a Cremer–Pople puckering amplitude of 0.892 Å. The HOMO–LUMO gap was 4.331 eV, with chemical hardness of 2.166 eV and electrophilicity of 3.241 eV. The molecule exhibits strong electrophilic and nucleophilic characteristics, with an electrostatic potential ranging from −38.0 to +45.3 kcal mol^{-1}.

Keywords: *1,3-Benzoxazepine; Schiff base; [2+5] cycloaddition; Isovanillin; Benzocaine; Density functional theory; Frontier molecular orbitals; Molecular electrostatic potential.*

***Corresponding Author**
Rawaa Naeamah Abdullah

DOI: https://doi.org/10.37022/jis.v9i2.149

Produced and Published by
South Asian Academic Publications

1. INTRODUCTION

Seven-membered rings that carry both oxygen and nitrogen occupy a curious position in heterocyclic chemistry. They are large enough to be conformationally flexible, which makes them harder to characterise than the corresponding five- and six-membered systems, and yet the 1,3-oxazepine framework appears in compounds with antibacterial, antifungal, anti-inflammatory, antitumour and antidepressant activity, and a recent review of multicomponent approaches to the ring makes clear that interest in it is still growing [1]. Other seven-membered nitrogen heterocycles, such as the triazepines and oxatriazepines, are being explored on the same basis [2]. The related oxazine and oxadiazole scaffolds have attracted similar attention as pharmacophores [3, 4].

The most widely used route to 1,3-oxazepine-4,7-diones is a two-step sequence. An aromatic aldehyde is first condensed with a primary aromatic amine to give a Schiff base, and the imine is then treated with a cyclic anhydride, usually maleic or phthalic, in a dry aprotic solvent under reflux [5–9]. The transformation is generally written as a [2+5] cycloaddition: the imine nitrogen and the anhydride combine so that the five-membered anhydride ring is opened and its two carbonyl carbons become, respectively, a lactam and a lactone carbon of the new seven-membered ring. Maleic anhydride delivers 1,3-oxazepine-4,7-diones with an intact ring C=C double bond, whereas phthalic anhydride delivers the benzo-fused analogues, described in the older literature as [1,3]oxazepine-1,5-diones and named here, following current fusion nomenclature, as 2,3-dihydro-1,3-benzoxazepine-4,9-diones [9, 10]. Tetrachlorophthalic anhydride behaves in the same way [11]. Reports on oxazepines obtained by this route describe antibacterial and antifungal

activity [11, 12]; related thiophene–thiazole and thiazolidinone Schiff base hybrids show the same profile [13, 14], antioxidant activity measured by DPPH and hydroxyl-radical scavenging [15, 16], and, in one recent study of sulfonamide-derived oxazepines, a combination of antimicrobial and antioxidant activity with low cytotoxicity supported by DFT and docking calculations [17]. Docking studies on bis-benzoxazepines against the progesterone receptor have also suggested anticancer potential [10].

Vanillin and its isomers are attractive aldehyde partners: inexpensive, obtainable from renewable sources, and the phenolic hydroxyl left after condensation contributes to hydrogen bonding and to radical scavenging [18–22]. Isovanillin, the 3-hydroxy-4-methoxy isomer, is used much less often than vanillin itself. Benzocaine (ethyl 4-aminobenzoate) is an equally convenient amine, with a para ester group that acts as a strong electron acceptor and leaves a handle for further functionalisation.

Quantum chemistry has become a routine companion to preparative work of this kind, and frontier-orbital energies, conceptual-DFT descriptors and electrostatic potential maps now appear alongside spectra in most papers of the type [17, 23–27]. In particular, phenolic Schiff bases and related heterocycles benefit from analyses of hydrogen-atom transfer and radical stabilisation based on frontier-orbital and electrostatic-potential arguments [26, 27]. We report here the synthesis and spectroscopic characterisation of ethyl 4-[2-(3-hydroxy-4-methoxyphenyl)-4,9-dioxo-2,3,4,9-tetrahydro-1,3-benzoxazepin-3-yl]benzoate together with a computational study covering geometry, vibrational frequencies, frontier orbitals, global descriptors, electrostatic potential, atomic charges and thermochemistry. Azomethines of this kind are also established precursors to six-membered 1,3-thiazinan-4-ones on treatment with 3-mercaptopropanoic acid [28], so the seven-membered oxygen/nitrogen ring reported here is one member of a small family of heterocycles that a single Schiff base makes available.

2. MATERIALS AND METHODS

2.1. Chemicals and instrumentation

Isovanillin (3-hydroxy-4-methoxybenzaldehyde, ≥99%), benzocaine (ethyl 4-aminobenzoate, ≥99%), phthalic anhydride (≥99%), absolute ethanol (99.9%), glacial acetic acid (99.8%), benzene (≥99.5%), ethyl acetate, toluene, n-hexane and anhydrous sodium sulfate were of analytical-reagent grade, supplied by Merck, BDH, Fluka and Sigma-Aldrich, and were used as received without further purification. Benzene was dried over anhydrous sodium sulfate for 24 h, decanted, distilled and stored over activated 4 Å molecular sieves; it is referred to below as dry benzene. Benzene is classified as a category 1A carcinogen (H350), so all operations involving it were carried out in an efficient fume hood with nitrile gloves and eye protection, and the residues were collected for licensed disposal.

The progress of both steps and the purity of the products were followed by thin-layer chromatography on Merck silica-gel 60 F_{254} aluminium-backed plates (layer thickness 0.20 mm). The condensation of Section 2.2 was developed with n-hexane/ethyl acetate 3:1 (v/v) and the cycloaddition of Section 2.3 with ethyl acetate/toluene 1:1 (v/v). A step was taken to be complete when the spot of the limiting starting material could no longer be detected and a single new spot of different R_f was obtained. Spots were visualised under ultraviolet light at 254 nm and, where required, by exposure to iodine vapour.

Melting points were determined in open capillaries on an Electrothermal 9100 digital melting-point apparatus (Bibby Scientific, Staffordshire, UK) and are uncorrected. Infrared spectra were recorded as KBr discs (about 2 mg of sample in 200 mg of spectroscopic-grade potassium bromide) over the 4000–400 cm^{-1} range at a resolution of 4 cm^{-1} with 32 accumulated scans on a Shimadzu FTIR-8400S Fourier-transform infrared spectrophotometer (Shimadzu Corporation, Kyoto, Japan). NMR spectra were obtained on a Bruker Avance spectrometer (Bruker BioSpin, Rheinstetten, Germany) operating at 300.81 MHz for ^1H and 75.65 MHz for ^{13}C, with DMSO-d_6 as solvent at 295–296 K and a sample concentration of about 10 mg in 0.6 mL. ^1H chemical shifts are referenced to internal tetramethylsilane at 0.00 ppm, and ^{13}C chemical shifts to the DMSO-d_6 septet at 39.52 ppm; the residual DMSO-d_5 proton signal, observed here at 2.52–2.53 ppm, is reported in the NMR data table of Section 3.3 but is not used as a reference. Coupling constants J are given in Hz, and the multiplicities are abbreviated s (singlet), d (doublet), t (triplet), q (quartet) and m (multiplet).

2.2. Ethyl 4-{[(3-hydroxy-4-methoxyphenyl) methylidene] amino} benzoate (1)

Isovanillin (1.52 g, 10.0 mmol, 1.0 equiv.) and benzocaine (1.65 g, 10.0 mmol, 1.0 equiv.) were dissolved separately in absolute ethanol (15 mL each). Three or four drops of glacial acetic acid (about 0.05 mL) were added to the aldehyde solution, which was then added dropwise over about ten minutes to the amine solution in a 100 mL round-bottomed flask fitted with a reflux condenser. The combined mixture (total volume 30 mL, 0.33 M in each reagent) was refluxed on a water bath at 78 °C for four hours with continuous magnetic stirring and the condensation was followed by TLC (n-hexane/ethyl acetate 3:1). After cooling slowly to room temperature and standing at 4 °C overnight the solid that separated was collected by filtration under suction, washed with cold absolute ethanol (3 × 5 mL) and recrystallised from hot absolute ethanol (about 25 mL) to give the title compound (1) as a yellow crystalline solid (2.54 g, 8.50 mmol, 85%). m.p. 148–150 °C. The product gave a single spot on TLC (n-hexane/ethyl acetate 3:1).

IR (KBr, cm^{-1}): 3463, 3369, 3241 (ν O–H, phenolic); 2976, 2936, 2843 (ν C–H, aliphatic); 1679 (ν C=O, ester); 1642 (ν C=N, azomethine); 1603, 1579, 1516 (ν

C=C, aromatic); 1440, 1369 (δ C–H); 1275, 1249, 1216, 1169, 1121 (ν C–O, ester and aryl ether); 864–767 (γ C–H, out-of-plane). ^{1}H NMR (300.81 MHz, DMSO-d_6, ppm): δ 9.82 (s, 1H, phenolic OH), 8.43 (s, 1H, CH=N), 7.99–6.64 (m, 7H, aromatic H), 4.33–4.17 (q, J = 7.1 Hz, 2H, OCH_2), 3.86 (s, 3H, OCH_3), 1.34–1.24 (t, J = 7.1 Hz, 3H, CH_3). ^{13}C NMR (75.65 MHz, DMSO-d_6, ppm): δ 165.94 (ester C=O), 162.09 (CH=N), 153.85, 151.83, 147.55–111.87 (aromatic C), 60.99 (OCH_2), 56.12 (OCH_3), 14.73 (CH_3). Calculated monoisotopic mass for $C_{17}H_{17}NO_4$: 299.1158; calculated $[M+H]^+$ 300.1230. Calculated elemental composition (M = 299.33 g mol^{-1}): C 68.22, H 5.72, N 4.68. Canonical SMILES: CCOC(=O)c1ccc(/N=C/c2ccc(OC)c(O)c2)cc1. InChIKey: NBEOIRKSZVWLNF-WOJGMQOQSA-N.

2.3. Ethyl 4-[2-(3-hydroxy-4-methoxyphenyl)-4,9-dioxo-2,3,4,9-tetrahydro-1,3-benzoxazepin-3-yl]benzoate (2)

A mixture of the Schiff base 1 (0.179 g, 0.598 mmol, 1.0 equiv.) and phthalic anhydride (0.240 g, 1.62 mmol, 2.71 equiv.) in dry benzene (20 mL) was heated under reflux, in a 50 mL round-bottomed flask fitted with a reflux condenser closed by a calcium chloride guard tube, on a water bath at 75–80 °C for 5 h with continuous magnetic stirring. An equimolar ratio is the usual choice for this cycloaddition [5–12]; the excess of anhydride was taken here because of the small scale on which the reaction was run, and it is removed in the work-up. The reaction was followed by TLC (ethyl acetate/toluene 1:1) and was stopped when the spot of 1 could no longer be detected. The mixture was cooled to room temperature and the benzene was removed under reduced pressure on a rotary evaporator at 40 °C. The residual coloured solid was triturated with cold absolute ethanol (3 × 5 mL), which takes up the unreacted phthalic anhydride together with the phthalic acid formed from it on contact with moisture, collected by filtration under suction, and recrystallised from ethyl acetate (about 10 mL). Drying to constant weight in a vacuum desiccator over anhydrous calcium chloride gave the title compound (2) as a yellow solid ([mass] g, [yield %]). m.p. [m.p. °C]. The product gave a single spot on TLC (ethyl acetate/toluene 1:1).

IR (KBr, cm^{-1}): 3213, 3113 (ν O–H, phenolic, hydrogen-bonded); 1709 (ν C=O, lactone and ester); 1674 (ν C=O, lactam); 1580, 1548, 1513 (ν C=C, aromatic); 1463, 1442, 1407 (δ C–H); 1365 (ν C–N, amide); 1278, 1176, 1155, 1120 (ν C–O, lactone, ester and aryl ether); 1021, 967, 866, 829, 791, 771 (γ C–H, out-of-plane); 695, 636, 609, 588, 503 (skeletal). ^{1}H NMR: the ^{1}H spectrum of 2 was not recorded in the present study; the consequence for the assignment of the N,O-acetal centre C-8 is set out in Section 3.3. ^{13}C NMR (75.65 MHz, DMSO-d_6, ppm): δ 174.92 (lactam C=O, C-9), 169.20 (lactone C=O, C-12), 166.37 (ester C=O, C-1), 156.51, 153.89, 151.85, 147.51 (oxygen-substituted aromatic C), 133.34, 131.52, 131.22, 130.89, 130.33, 129.32, 128.88 (fused benzo and aromatic CH), 124.89–112.03 (aromatic C), 61.05 (OCH_2, C-24), 56.23 (OCH_3, C-23), 14.81 (CH_3, C-25); the N,O-acetal carbon C-8 was not observed (see Section 3.3). Calculated monoisotopic mass for $C_{25}H_{21}NO_7$: 447.1318; calculated $[M+H]^+$ 448.1391. Calculated elemental composition (M = 447.44 g mol^{-1}): C 67.11, H 4.73, N 3.13. Canonical SMILES: CCOC(=O)c1ccc(N2C(=O)c3ccccc3C(=O)OC2c2ccc(OC)c(O)c2)cc1. InChIKey: GXTRIEWFUZTOOX-UHFFFAOYSA-N.

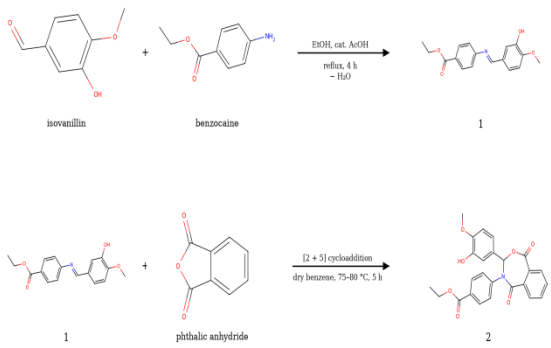

Figure 01: Two-step synthetic route to the title compound (2) through the Schiff base (1).

2.4. Computational details

All density-functional calculations were performed with the PySCF program package (version 2.14.0) [29]. The three-dimensional structure of 2 was generated from the canonical SMILES string given in Section 2.3 with the ETKDGv3 distance-geometry algorithm as implemented in RDKit; sixty conformers were requested (random seed 42, RMSD pruning threshold 0.5 Å), forty-one of which survived pruning and were relaxed with the MMFF94 force field. The six lowest-energy structures were then fully optimised with the semi-empirical tight-binding method GFN2-xTB [30] as implemented in the tblite library, using an analytic-gradient L-BFGS minimisation converged to a maximum residual gradient below 1.5 × 10^{-4} Hartree Bohr^{-1}. The six optimised conformers span only 0.68 kcal mol^{-1} and differ essentially in the orientation of the terminal ethyl and methoxy groups; the lowest of them, at −95.67682 Hartree, was taken as the working geometry.

An analytic B3LYP/6-31G(d) Hessian, and therefore a vibrationally verified B3LYP geometry optimisation, was beyond the computing budget available for the present study: with 504 contracted Gaussian functions for the 54 atoms a single self-consistent-field cycle already costs of the order of one and a half minutes on the hardware used here, so a full DFT optimisation followed by an analytic second-derivative calculation was not attainable. The protocol adopted instead, and used consistently throughout this work, is B3LYP/6-31G(d)//GFN2-xTB: the geometry, the harmonic frequencies, the infrared intensities and the rigid-rotor/harmonic-oscillator thermochemical corrections

are all obtained at the GFN2-xTB level, and the electronic structure — orbital energies, conceptual-DFT descriptors, electrostatic potential, atomic charges and vertical excitations-is obtained from a B3LYP/6-31G(d) calculation at that geometry. All wavenumbers and thermochemical values reported below are therefore semi-empirical and are quoted unscaled. Analytical B3LYP/6-31G(d) frequencies and continuum-solvation single-point energies at B3LYP/6-311++G(d,p) are planned for follow-up work and will be reported separately once the required resources are secured.

The harmonic force constants were obtained by central differences of the analytic GFN2-xTB gradient with a Cartesian displacement of 0.005 Å. The mass-weighted Hessian was projected onto the space orthogonal to the six translational and rotational degrees of freedom before diagonalisation; infrared intensities were obtained from numerical dipole derivatives taken along each normalised normal coordinate with a displacement of 0.01 Bohr and are reported relative to the strongest band. Thermochemical quantities were evaluated at 298.15 K and 1 atm within the rigid-rotor/harmonic-oscillator model with a rotational symmetry number of one.

The single-point electronic-structure calculation used the resolution-of-the-identity approximation for the Coulomb term (auxiliary basis def2-universal-jkfit), a level-3 exchange–correlation grid and an SCF convergence threshold of 10^{-9} Hartree. Global reactivity descriptors were obtained from the frontier-orbital energies within Koopmans' approximation: $I = -E(HOMO)$, $A = -E(LUMO)$, electronegativity $\chi = (I + A)/2$, chemical potential $\mu = -\chi$, chemical hardness $\eta = (I - A)/2$, global softness $\sigma = 1/(2\eta)$, electrophilicity index $\omega = \mu^2/(2\eta)$, and maximum charge transfer $\Delta N_{max} = -\mu/\eta$. The nucleophilicity index N was computed as $N = E(HOMO) - E(HOMO)_{TCE}$ using E(HOMO)TCE = −9.12 eV (−0.3351 a.u.; tetracyanoethylene optimised at B3LYP/6-31G(d), the value that underlies the original definition of Domingo) [31]. The classification of the electrophilicity value used the scale calibrated at B3LYP/6-31G(d) in the gas phase, that is, at the same level of theory as the calculation reported here [32]; the classification of the nucleophilicity value followed the parallel N-scale. On this scale $\omega > 1.5$ eV corresponds to a strong electrophile and $N > 3.0$ eV to a strong nucleophile; $\omega > 4.0$ eV and $N > 4.0$ eV correspond to the super classifications. Because these thresholds are level-of-theory dependent [32], we quote the original values and use them consistently.

The molecular electrostatic potential was computed directly from the converged first-order density matrix rather than from point charges, and was evaluated on the $\rho = 0.001$ a.u. electron-density isosurface. Atomic charges were obtained from Mulliken and meta-Löwdin population analyses so that the two partitioning schemes could be compared, and the frontier orbitals were decomposed over four molecular fragments by Mulliken partitioning of the orbital population.

3. RESULTS AND DISCUSSION

3.1. Synthesis

The two steps proceed as literature on related systems would suggest (Fig. 1). Condensation of isovanillin with benzocaine is fast under acid catalysis and the imine precipitates on cooling. The second step is the [2+5] cycloaddition of phthalic anhydride across the azomethine bond [5–9]. Mechanistically the imine nitrogen attacks one of the two anhydride carbonyl carbons, and the carboxylate generated by opening of the five-membered anhydride ring then closes onto the former azomethine carbon, so that one anhydride carbonyl becomes the lactam carbonyl C-9 and the other becomes the lactone carbonyl C-12 of the seven-membered ring. No small molecule is lost in this step, and the product is therefore the simple 1:1 adduct of 1 and phthalic anhydride, $C_{25}H_{21}NO_7$, a point that the mass balance confirms: 299.33 + 148.12 = 447.44 g mol^{-1}. The same sequence with maleic anhydride would give the non-fused 1,3-oxazepine-4,7-dione carrying a ring C=C double bond instead [6, 9], and with 3-mercaptopropanoic acid azomethines of this kind give six-membered 1,3-thiazinan-4-ones [28].

The atom numbering used throughout the spectroscopic and computational discussion is defined on the structure drawn alongside the ^{13}C NMR spectrum of 2 and is used consistently for the calculated structural parameters and atomic charges so that experiment and theory can be compared directly. Because compounds 1 and 2 have different heavy-atom counts, their atom numberings are independent, and identical labels can refer to different atoms in the two compounds. For compound 2 the ring atoms of the 1,3-benzoxazepine are also given in the standard heterocyclic numbering (O1, C2, N3, C4, C4a, C8a, C9, with C2 the N,O-acetal carbon, C4 the lactam carbonyl and C9 the lactone carbonyl) in the table of calculated structural parameters of Section 3.4, to avoid any ambiguity between the two conventions.

3.2. Infrared spectra

The infrared spectrum of the Schiff base 1 (Fig. 2) shows the features expected from a successful condensation. The pair of N–H stretching bands of benzocaine has disappeared, and a new sharp absorption is present at 1642 cm^{-1}, assigned to the azomethine C=N stretch. The phenolic O–H of the isovanillin fragment gives a broad band at 3369 cm^{-1} with weaker components at 3463 and 3241 cm^{-1}, and the ester carbonyl of the benzocaine fragment absorbs at 1679 cm^{-1}. Aromatic ring stretching appears at 1603, 1579 and 1516 cm^{-1}, the C–O stretches of the ester and the aryl ethers between 1275 and 1121 cm^{-1}, and the out-of-plane C–H deformations of the two para- and 1,3,4-trisubstituted rings between 864 and 767 cm^{-1}.

In the spectrum of the benzoxazepine 2 (Fig. 3) the band at 1642 cm^{-1} has disappeared, which is the clearest single piece of evidence that the C=N double bond is no longer present. In its place two carbonyl absorptions are now observed where the Schiff base

had only one. The strong band at 1709 cm^{-1} is assigned to the lactone carbonyl C-12 of the new ring, and the band at 1674 cm^{-1} to the lactam carbonyl C-9. A separation of 35 cm^{-1} between the two is what one expects when an ester-type and an amide-type carbonyl are placed on the same seven-membered ring: the lactam carbonyl is lowered by amide resonance, in which the nitrogen lone pair is delocalised onto the carbonyl oxygen and the C=O bond order is correspondingly reduced, whereas the lactone carbonyl retains a higher force constant because the ring oxygen is a much weaker π donor. The ester carbonyl of the benzoate fragment is a spectator in this reaction and is not resolved from the lactone band; both fall inside the strong envelope centred at 1709 cm^{-1}, which is consistent with the calculated pattern discussed below, where the lactone and ester modes lie only 17 cm^{-1} apart while the lactam mode is a further 23 cm^{-1} lower. The disappearance of the azomethine band together with the appearance of these two new carbonyl absorptions provides three consistent vibrational markers of ring formation.

The behaviour of the phenolic O–H is striking. In 1 it appears at 3369 cm^{-1}; in 2 it has moved to 3213 and 3113 cm^{-1}, a shift of roughly 200 cm^{-1} to lower wavenumber. A displacement of that size indicates a considerably stronger and more ordered hydrogen-bonded network in the solid, which is easy to rationalise: the product now offers three carbonyl oxygens as acceptors instead of two, and two of them, the lactam and lactone oxygens, sit on the same ring. A band at 1365 cm^{-1} is assigned to the C–N stretch of the newly formed amide linkage, and the C–O stretches of the lactone, the ester and the aryl ethers are found at 1278, 1176, 1155 and 1120 cm^{-1}. The out-of-plane C–H deformations at 771 and 695 cm^{-1} are characteristic of an ortho-disubstituted benzene ring and are absent from the spectrum of 1; they are the direct fingerprint of the phthalic fragment that has been incorporated.

Table 01 compares the calculated harmonic wavenumbers with the measured positions for compound 2. Leaving aside the O–H stretch, which the gas-phase calculation necessarily places too high because it describes a free rather than a hydrogen-bonded hydroxyl, the semi-empirical GFN2-xTB Hessian reproduces the position of each measured fingerprint band to within 47 cm^{-1} and most of them to within 20 cm^{-1}. Over the twenty-four fingerprint bands the mean absolute deviation is 17 cm^{-1}, with an RMSD of 21 cm^{-1} and an optimum linear scaling factor of 0.992. A Pearson correlation coefficient is not quoted, because with a wavenumber range spanning about 1200 cm^{-1} any linear regression of calculated on measured values gives $R > 0.99$ regardless of the size of the individual deviations; the MAD and RMSD give a more informative measure of agreement. The three carbonyl modes deserve particular comment. The calculation places them at 1755, 1739 and 1715 cm^{-1} and identifies them, from the atomic displacements, as the lactone, the ester and the lactam stretch respectively. That ordering is exactly the one inferred from the experimental spectrum, and the calculated lactone-to-lactam separation of 40 cm^{-1} is close to the 35 cm^{-1} measured between the 1709 and 1674 cm^{-1} bands. The systematic overestimate of about 40 cm^{-1} for all three is the expected behaviour of an unscaled semi-empirical harmonic Hessian for carbonyl stretches, which are also the modes most affected by the intermolecular hydrogen bonding present in the KBr disc but absent from the gas-phase calculation.

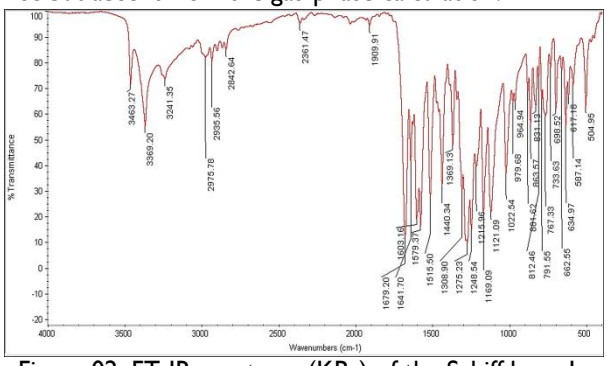

Figure 02: FT-IR spectrum (KBr) of the Schiff base 1.

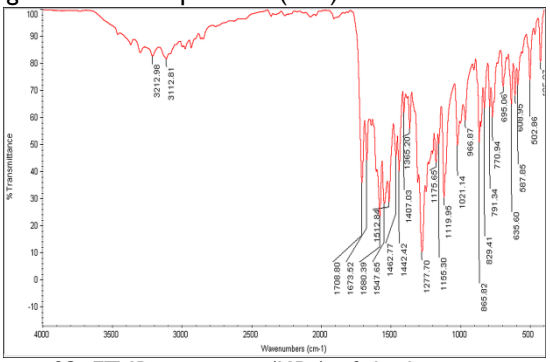

Figure 03: FT-IR spectrum (KBr) of the benzoxazepine 2.

Table 01: Characteristic infrared bands of compound 2: measured wavenumbers (KBr, cm^{-1}) compared with the calculated harmonic values (GFN2-xTB, unscaled).

Assignment	Experimental	Calculated	Calc. – exp.
ν(O-H) phenolic	3213, 3113	3478.5	—
ν(C=O) lactone	1709 (s)	1755.5	+46.5
ν(C=O) ester	1709 (s)	1738.5	+29.5
ν(C=O) lactam	1674 (m)	1715.1	+41.1
ν(C=C) aromatic	1580	1589.3	+9.3
ν(C=C) aromatic	1548	1585.4	+37.4
ν(C=C) aromatic	1513	1499.5	-13.5

Assignment	Experimental	Calculated	Calc. – exp.
δ(C-H) in-plane	1463	1473.9	+10.9
δ(C-H) in-plane	1442	1443.7	+1.7
δ(C-H) in-plane	1407	1409.7	+2.7
ν(C-N) amide	1365	1347.4	-17.6
ν(C-O) lactone / ester	1278	1300.3	+22.3
ν(C-O) aryl ether	1176	1182.1	+6.1
ν(C-O) methoxy	1155	1126.2	-28.8
ν(C-O) phenol	1120	1121.1	+1.1
ring breathing / ν(C-O)	1021	1052.4	+31.4
γ(C-H) out-of-plane	967	957.9	-9.1
γ(C-H) out-of-plane	866	850.9	-15.1
γ(C-H) out-of-plane	829	824.5	-4.5
γ(C-H) out-of-plane	791	798.0	+7.0
γ(C-H) ortho-benzo	771	787.7	+16.7
γ(C-H) ortho-benzo	695	688.7	-6.3
skeletal deformation	636	662.5	+26.5
skeletal deformation	588	589.3	+1.3
skeletal deformation	503	482.9	-20.1

The O–H entry carries no deviation because the calculation describes a free hydroxyl whereas the measured band is that of a hydrogen-bonded one in the solid; it is excluded from the statistics quoted in the text.

3.3. NMR spectra

The ^{1}H NMR spectrum of 1 (Fig. 4) shows the azomethine proton as a singlet at 8.43 ppm, the phenolic hydroxyl at 9.82 ppm, and the aromatic protons of the two rings spread between 7.99 and 6.64 ppm. The ethyl ester gives the expected pattern, a quartet centred at 4.25 ppm for the OCH_2 group and a triplet at 1.31 ppm for the methyl, and the aromatic methoxy group appears as a singlet at 3.86 ppm. The residual solvent signal falls at 2.53 ppm. The full data set for both compounds is collected in Table 2.

The ^{13}C spectrum of 1 (Fig. 5) supports the same conclusion. The azomethine carbon C-8 resonates at 162.09 ppm and the ester carbonyl C-1 at 165.94 ppm. The two oxygen-bearing aromatic carbons give signals at 153.85 and 151.83 ppm, the remaining aromatic carbons fall between 147.55 and 111.87 ppm, and the aliphatic region contains the OCH_2 carbon at 60.99 ppm, the methoxy carbon at 56.12 ppm and the ester methyl at 14.73 ppm. A weak resonance at 191.76 ppm is the aldehyde carbon of a small amount of unconsumed isovanillin.

After cycloaddition the low-field region changes in a diagnostic way. In the ^{13}C spectrum of 2 (Fig. 6) the azomethine signal at 162.09 ppm has been replaced by two new carbonyl resonances at 174.92 and 169.20 ppm, while the ester carbonyl of the benzoate fragment is essentially unmoved at 166.37 ppm. The appearance of three carbonyl carbons where the precursor had one, together with the loss of the azomethine carbon, is the most direct piece of evidence for the seven-membered ring, and neither new signal can arise from unreacted starting material. We assign the resonance at 174.92 ppm to the lactam carbonyl C-9 and that at 169.20 ppm to the lactone carbonyl C-12, following the usual ordering in which an amide carbonyl resonates to lower field than the corresponding ester; the assignment should, however, be regarded as tentative, because the calculated atomic charges of Section 3.8 put the lactone carbon slightly ahead of the lactam carbon in positive charge, and a firm individual attribution would require a two-dimensional experiment such as HMBC. The aromatic region is correspondingly more crowded: signals at 133.34, 131.52, 131.22, 130.89, 130.33, 129.32 and 128.88 ppm are new relative to 1 and belong to the four methine carbons and the two ring-fusion carbons of the phthalic-derived benzo ring. The OCH_2 carbon at 61.05 ppm (C-24), the methoxy carbon at 56.23 ppm (C-23) and the ester methyl at 14.81 ppm (C-25) are found where they were in 1, as expected for a fragment that takes no part in the reaction.

One point must be stated plainly rather than glossed over. The N,O-acetal carbon C-8 of the new ring, that is, the carbon that was the azomethine carbon of 1 and is now an sp^3 centre flanked by the ring nitrogen and the ring oxygen, is expected on the basis of related 2,3-dihydro-1,3-benzoxazepines to resonate between about 80 and 90 ppm. No signal is observed in the 65–110 ppm window of the spectrum recorded here, which is flat at the noise level throughout that region. Three explanations are possible: the resonance is a single protonated carbon of long relaxation time and low intensity that has not been accumulated with a sufficient number of transients; it is broadened beyond detection by slow conformational exchange of the flexible seven-membered ring, a mechanism for which the calculated twist-boat geometry of Section 3.4

provides an obvious basis; or the ring has not in fact closed at that carbon. The first two are consistent with the infrared evidence and with the two new carbonyl resonances, but the third cannot be excluded on the present data alone. A ^{13}C spectrum recorded with a substantially larger number of scans, together with DEPT-135 and HSQC experiments and a ^{1}H spectrum of the purified product, would settle the question directly by locating the methine carbon and correlating it with its attached proton, and these measurements are recommended before the structure is regarded as fully proven.

Minor signals in the ^{13}C spectrum of 2 at 195.33 and 191.91 ppm, and the doubling seen at 166.37/165.95, 61.05/59.95, 56.23/56.09 and 14.81/14.65 ppm, correspond to trace amounts of residual isovanillin and of unreacted Schiff base 1 carried through the recrystallisation. They are reported here for completeness and are not used in the assignments.

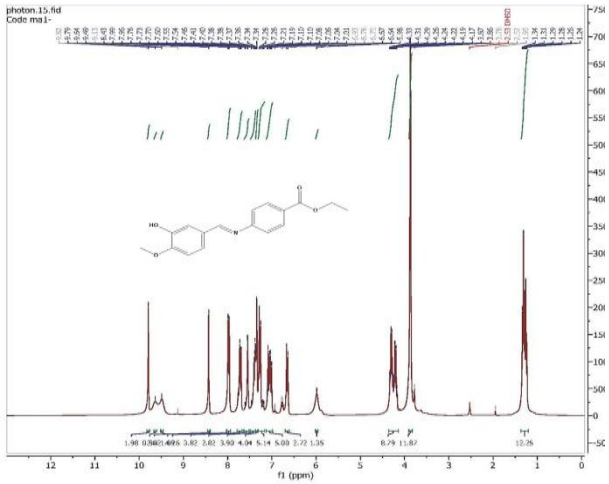

Figure 04: ^{1}H NMR spectrum (300.81 MHz, DMSO-d_6) of the Schiff base 1.

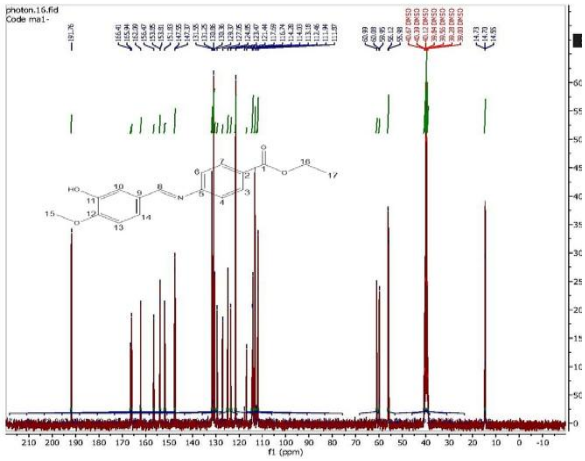

Figure 05: ^{13}C NMR spectrum (75.65 MHz, DMSO-d_6) of the Schiff base 1, with the atom numbering used in the text.

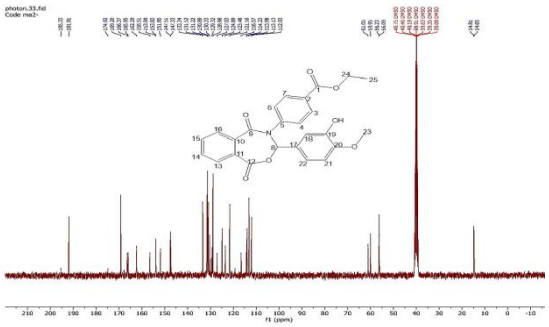

Figure 06: ^{13}C NMR spectrum (75.65 MHz, DMSO-d_6) of the benzoxazepine 2, with the atom numbering used in the text and in the computational tables.

Table 02: ^{1}H and ^{13}C NMR data for compounds 1 and 2 (DMSO-d_6, chemical shifts in ppm).

Cmpd	Nucleus	δ (ppm)	Mult.	Assignment
1	^{1}H	9.82	s	OH (phenolic)
1	^{1}H	8.43	s	CH=N (H-8)
1	^{1}H	7.99–6.64	m	aromatic H
1	^{1}H	4.33–4.17	q	OCH_2 (H-16)
1	^{1}H	3.86	s	OCH_3 (H-15)
1	^{1}H	2.53	—	DMSO-d_6
1	^{1}H	1.34–1.24	t	CH_3 (H-17)
1	^{13}C	165.94	—	C-1, ester C=O
1	^{13}C	162.09	—	C-8, CH=N
1	^{13}C	153.85, 151.83	—	oxygenated aromatic C
1	^{13}C	147.55–111.87	—	aromatic C
1	^{13}C	60.99	—	C-16, OCH_2
1	^{13}C	56.12	—	C-15, OCH_3
1	^{13}C	14.73	—	C-17, CH_3
2	^{1}H	not recorded		see Section 3.3
2	^{13}C	174.92	—	C-9, lactam C=O
2	^{13}C	169.20	—	C-12, lactone C=O
2	^{13}C	166.37	—	C-1, ester C=O
2	^{13}C	156.51, 153.89, 151.85, 147.51	—	oxygenated aromatic C
2	^{13}C	133.34–	—	fused benzo

Cmpd	Nucleus	δ (ppm)	Mult.	Assignment
		128.88		C
2	^{13}C	124.89–112.03	—	aromatic C
2	^{13}C	61.05	—	C-24, OCH_2
2	^{13}C	56.23	—	C-23, OCH_3
2	^{13}C	14.81	—	C-25, CH_3
2	^{13}C	not observed	—	C-8, N,O-acetal CH (expected 80–90 ppm)

3.4. Optimised molecular geometry

The optimised structure is shown in Fig. 7 and the more informative parameters are collected in Table 3. The molecule is built from four units: the ethyl benzoate ring attached to the ring nitrogen, the seven-membered 1,3-benzoxazepine-4,9-dione core, the benzo ring fused to it, and the 3-hydroxy-4-methoxyphenyl (guaiacyl) substituent at the sp^3 ring carbon.

The seven-membered ring is neither planar nor a simple boat. All seven endocyclic torsion angles are given in Table 3, and the puckering is quantified by the Cremer–Pople coordinates [33] computed from the optimised coordinates: the total puckering amplitude Q is 0.892 Å, and the decomposition into ring-puckering modes gives q_2 = 0.876 Å and q_3 = 0.168 Å with ϕ_2 = 77.9°. The dominance of the two-fold amplitude q_2 over q_3 by a factor of five identifies the conformation as a twist-boat rather than a chair-like or a symmetric boat form. The two torsions on either side of the sp^3 carbon, O1–C2–N3–C4 = 72.1° and C9–O1–C2–N3 = -71.6°, are large and of opposite sign, whereas the three torsions that involve the rigid benzo fusion are small (C2–N3–C4–C4a = 2.2°, C4–C4a–C8a–C9 = 3.3°, C8a–C9–O1–C2 = -1.4°). The puckering is therefore concentrated almost entirely at C2, which lies 0.558 Å out of the mean plane of the ring while no other ring atom deviates by more than 0.37 Å. This is exactly what the connectivity requires: the fused benzo ring locks four consecutive ring atoms into a plane, so the only degree of freedom left to relieve strain is the carbon that carries the aryl group. The sum of the seven endocyclic torsions is 1.3°, close to the zero expected for a closed ring, which is a useful internal check on the optimisation.

The amide fragment is planar. The improper torsion O4=C4(–N3)(–C4a) is 179.1°, and the three angles at nitrogen sum to 359.6°, so N3 is essentially sp^2 despite carrying three substituents. The N3–C4 distance of 1.3734 Å is about 0.09 Å shorter than a normal N–C single bond, the familiar signature of amide resonance and a clear indication that delocalisation across the N3–C4=O4 unit is effective. Consistently, the N3–C2 bond to the sp^3 carbon is long at 1.4430 Å.

The two ring carbonyls differ in a way that matches the infrared and NMR data. The lactam C4=O distance is 1.2108 Å and the lactone C9=O distance is 1.2007 Å, so the lactam carbonyl is the longer and therefore the weaker of the two, which is the geometric counterpart of its lower stretching wavenumber. The lactone C9–O1 bond of 1.3516 Å is short for a C–O single bond and reflects the usual ester-type conjugation, while the O1–C2 bond on the other side of the ring oxygen is a normal 1.4180 Å. The ester carbonyl of the benzoate fragment, at 1.2076 Å, is intermediate and essentially unchanged from its value in the Schiff base.

The relative orientation of the three ring systems is the other notable feature. The benzoate ring is nearly coplanar with the fused benzo ring, the angle between the two planes being only 6.2°, whereas the guaiacyl ring is turned away from both, by 39.7° from the benzo ring and by 34.1° from the benzoate ring. The N-aryl twist, measured by the C4–N3–C(aryl)–C(ortho) torsion, is 50.6° from coplanarity. The ester group is coplanar with its own ring (-0.7°), so conjugation with the benzene ring is preserved, and the methoxy group is likewise coplanar with the guaiacyl ring (-0.2°). The C–OH bond of the phenol (1.3534 Å) is shorter than either C–O bond of the methoxy group (1.3718 and 1.4074 Å), consistent with stronger π donation from the hydroxyl oxygen. The phenolic hydrogen sits 2.13 Å from the methoxy oxygen, a distance short enough for the weak intramolecular O–H···OCH_3 contact characteristic of guaiacol-type rings, which competes with the intermolecular hydrogen bonding seen in the solid-state infrared spectrum.

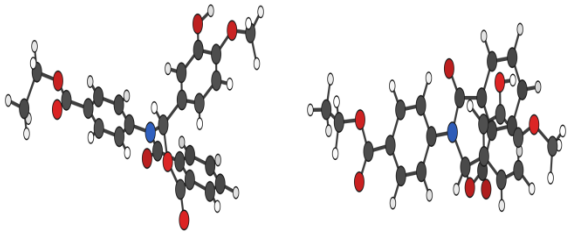

Figure 07: GFN2-xTB optimised structure of compound 2 in two orthogonal orientations. Carbon grey, hydrogen white, nitrogen blue, oxygen red.

Table 03: Selected calculated bond lengths (Å), bond angles and torsion angles (degrees) of compound 2. The first column uses the standard 1,3-benzoxazepine ring numbering, the second the atom labels of Fig. 06.

Parameter	Atoms (Fig. 6)	Calculated value
C=O (ester)	C1–O3	1.2076
C–O (ester)	C1–O2	1.3393
O–CH_2	O2–C24	1.4268
C=O (lactam, C4 of ring)	C9–O4	1.2108
C=O (lactone, C9 of ring)	C12–O5	1.2007

Parameter	Atoms (Fig. 6)	Calculated value
N3–C4 (amide)	N3–C9	1.3734
N3–C2 (N,O-acetal)	N3–C8	1.4430
N3–C(aryl)	N3–C5	1.4182
O1–C2 (ring)	O1–C8	1.4180
O1–C9 (ring lactone)	O1–C12	1.3516
C4–C4a (ring)	C9–C10	1.4936
C9–C8a (ring)	C12–C11	1.4892
C4a–C8a (fusion bond)	C10–C11	1.3974
C2–C(aryl)	C8–C17	1.5174
C–OCH_3	C20–O6	1.3718
O–CH_3	O6–C23	1.4074
C–OH	C21–O7	1.3534
aryl–C(ester)	C2–C1	1.4836
C2–N3–C4	C8–N3–C9	121.37
C(aryl)–N3–C2	C5–N3–C8	118.12
C(aryl)–N3–C4	C5–N3–C9	120.08
N3–C2–O1	N3–C8–O1	110.65
C2–O1–C9	C8–O1–C12	120.45
O1–C9–C8a	O1–C12–C11	118.58
N3–C4–C4a	N3–C9–C10	116.24
N3–C2–C(aryl)	N3–C8–C17	113.03
O1–C2–C(aryl)	O1–C8–C17	113.50
ring torsion O1–C2–N3–C4	—	72.10
ring torsion C2–N3–C4–C4a	—	2.16
ring torsion N3–C4–C4a–C8a	—	-44.99
ring torsion C4–C4a–C8a–C9	—	3.33
ring torsion C4a–C8a–C9–O1	—	41.69
ring torsion C8a–C9–O1–C2	—	-1.43
ring torsion C9–O1–C2–N3	—	-71.57
sum of endocyclic torsions	—	1.27
N-aryl ring twist (Ar vs amide plane)	C9–N3–C5–C6	-129.40
ester coplanarity (benzoate)	O3–C1–C2–C3	-0.72
amide planarity (improper)	O4=C9(N3)(C10)	179.13
Cremer–Pople puckering amplitude	Q (seven-membered ring)	0.892 Å
Cremer–Pople two-fold amplitude	q_2	0.876 Å
Cremer–Pople three-fold amplitude	q_3	0.168 Å
Cremer–Pople phase angle	ϕ_2	77.9°
largest deviation from the mean ring plane	C2 (C8)	0.558 Å

3.5. Frontier molecular orbitals and density of states

Frontier-orbital isosurfaces are shown in Fig. 8, the corresponding energy-level diagram in Fig. 9, and the energies are listed in Table 4. To make the description quantitative rather than visual, the molecule was divided into four fragments-the ethyl benzoate group, the seven-membered ring with its two carbonyls, the fused benzo ring, and the guaiacyl group-and the Mulliken population of each frontier orbital was partitioned among them.

The result is a clean donor–acceptor separation. The HOMO, at -5.912 eV, is 91.6% localised on the guaiacyl ring, with the hydroxyl and methoxy oxygen lone pairs contributing to the π system; contributions from every other fragment are below 7%. The LUMO, at -1.581 eV, lies almost entirely on the other side of the molecule: 50.6% on the fused benzo ring, 31.7% on the seven-membered ring, chiefly on the two carbonyl groups, and only 7.7% on the guaiacyl ring. In other words the phthaloyl-derived unit, and not the ethyl benzoate, is the electron acceptor of this molecule. The benzoate group carries the next orbitals on both sides: HOMO−1 is 53.3% and LUMO+1 is 62.7% benzoate in character.

The resulting gap is 4.331 eV, and the frontier-orbital decomposition shows where it comes from: the lactam and lactone carbonyls of the new ring, reinforced by the fused benzo ring, provide the π acceptor level that becomes the LUMO, while the HOMO sits on the guaiacyl donor at the other end of the molecule. The gap remains wide by the standards of conjugated Schiff bases, where values of roughly 3.8–4.1 eV have been

reported at comparable DFT levels [34], which is expected because the sp^3 carbon C2 interrupts conjugation between donor and acceptor; the molecule behaves electronically as a donor and an acceptor joined by an insulating bridge rather than as one extended chromophore. A gap of this size is usually read as an indicator of kinetic stability and is consistent with the observation that the product is an easily handled crystalline solid.

The orbitals immediately below the HOMO are well separated from it, HOMO−1 lying 0.59 eV lower at -6.507 eV and HOMO−2 0.74 eV lower at -6.657 eV, whereas on the virtual side LUMO+1 sits only 0.37 eV above the LUMO at -1.216 eV and LUMO+2 a further 0.30 eV higher. That asymmetry matters for the absorption spectrum, because several close-lying acceptor orbitals can be reached from the same donor orbital. The density of states in Fig. 10 shows the same thing in a different form: a dense band of occupied levels between −12 and −6 eV, a clear gap, then a set of virtual levels beginning near −2 eV.

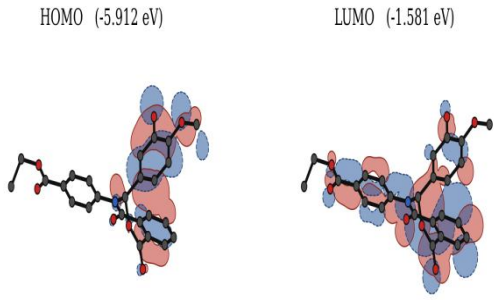

Figure 08: Isosurface plots (±0.02 a.u.) of the HOMO and the LUMO of compound 2. Red and blue denote opposite phases of the wavefunction.

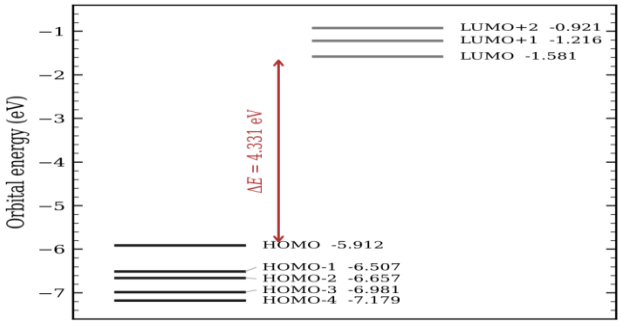

Figure 09: Energy-level diagram of the orbitals around the frontier region.

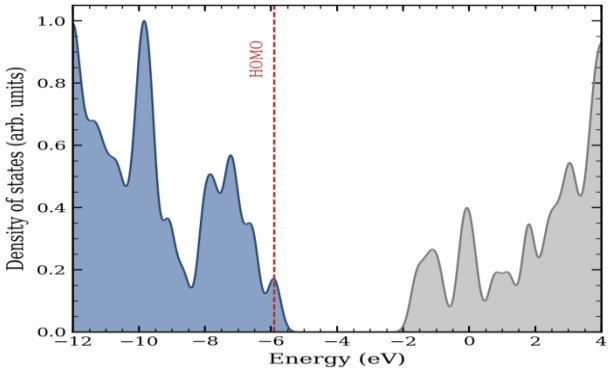

Figure 10: Total density of states. The dashed line marks the HOMO level.

Table 04: Frontier-orbital energies, fragment composition and total electronic energy at B3LYP/6-31G(d)//GFN2-xTB.

Orbital / quantity	Value	Dominant fragment (%)
E(LUMO+2)	-0.9208 eV	—
E(LUMO+1)	-1.2160 eV	ethyl benzoate 62.7
E(LUMO)	-1.5811 eV	fused benzo 50.6; ring 31.7
E(HOMO)	-5.9125 eV	guaiacyl 91.6
E(HOMO−1)	-6.5070 eV	ethyl benzoate 53.3
E(HOMO−2)	-6.6571 eV	guaiacyl 55.8
Energy gap, ΔE	4.3314 eV	—
Total electronic energy	-1546.603142 Hartree	—
Number of basis functions	504	—

3.6. Global reactivity descriptors

The global descriptors derived from the frontier energies are collected in Table 5 and compared graphically in Fig. 11. The ionisation potential of 5.912 eV and the electron affinity of 1.581 eV give an electronegativity of 3.747 eV and a chemical potential of −3.747 eV. The chemical hardness is 2.166 eV and the corresponding global softness 0.231 eV^{-1}.

The electrophilicity index ω = 3.241 eV places the compound in the strong-electrophile range (ω > 1.5 eV) on the scale of Domingo, Ríos-Gutiérrez and Pérez [31], calibrated at B3LYP/6-31G(d) in the gas phase [32], which is the same level of theory used here. On the parallel N-scale, the nucleophilicity index N = 3.205 eV, referenced to tetracyanoethylene (E(HOMO)TCE = −9.12 eV at B3LYP/6-31G(d)), places the molecule in the strong-nucleophile range (N > 3.0 eV), though not far above the threshold. Neither value exceeds the "super" threshold of 4.0 eV. The simultaneous appearance of strong-electrophile and strong-nucleophile character is not a contradiction on the Domingo scheme, since the two indices are not simple inverses of one another; it in fact reinforces the description of a molecule with spatially separated donor and acceptor sub-units (Section 3.5). The level-of-theory dependence of the Domingo thresholds has been quantified [32], which is why we retain here the original B3LYP/6-31G(d) thresholds consistent with our own level of theory.

The descriptors are consistent with the way the molecule is built. Three carbonyl acceptors, a lactone, a lactam and an ester, together with the fused aromatic ring, hold the LUMO at the phthaloyl end, while the HOMO stays on the guaiacyl donor. The hardness of 2.166 eV and the electrophilicity index of 3.241 eV therefore describe a soft and strongly electrophilic molecule whose nucleophilic character, N = 3.205 eV,

originates on a different fragment altogether. Being a strong electrophile and a strong nucleophile at the same time is what is expected when the accepting and donating roles are carried by separate parts of one structure.

The maximum charge transfer ΔN_{max} = 1.730 is a formal Koopmans-derived index rather than a physical electron count. Its value places the present compound within the range reported for structurally related oxazepines, thiazoles and Schiff bases examined as antioxidants and corrosion inhibitors [17, 25, 34–36]. The calculated dipole moment of 7.574 D is large for a neutral molecule of this size and deserves comment: the two ring carbonyls point in a similar direction and add to the amide dipole instead of cancelling it, so the individual bond moments reinforce rather than oppose one another. A dipole of this size implies appreciably greater solubility in polar media and stronger electrostatic steering in any binding event.

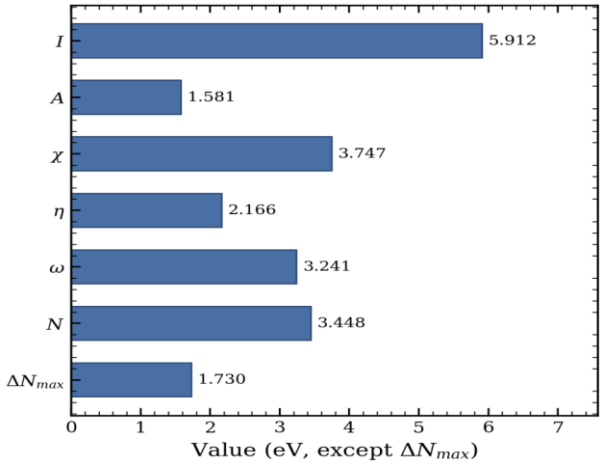

Figure 11: Calculated global reactivity descriptors.

Table 05: Conceptual-DFT global reactivity descriptors from the frontier-orbital energies within Koopmans' approximation.

Descriptor	Symbol	Value	Unit
Ionisation potential	I	5.9125	eV
Electron affinity	A	1.5811	eV
Electronegativity	χ	3.7468	eV
Chemical potential	μ	-3.7468	eV
Chemical hardness	η	2.1657	eV
Global softness	σ	0.2309	eV^{-1}
Electrophilicity index	ω	3.2410	eV
Nucleophilicity index	N	3.2045	eV
Maximum charge transfer	ΔN_{max}	1.7300	—
Dipole moment	μ_{el}	7.5745	Debye

3.7. Molecular electrostatic potential

The electrostatic potential evaluated on the ρ = 0.001 a.u. isodensity surface is shown in Fig. 12. Values run from -0.0606 to +0.0721 a.u., that is from −38.0 to +45.3 kcal mol^{-1}. The deepest minimum sits above the lactone carbonyl oxygen O5 of the seven-membered ring, with the lactam oxygen O4 and the ester oxygen O3 following closely; these three carbonyl oxygens together define the whole negative face of the molecule. They are the sites where an electrophile, a proton or a metal ion would attach first, and they are also the strongest hydrogen-bond acceptors available. The infrared data support this reading directly: the phenolic O–H stretch of 2 is about 200 cm^{-1} lower than in 1, which is what one expects if the hydroxyl is engaged in a strong intermolecular hydrogen bond to a carbonyl oxygen in the solid state, and the compound offers three such acceptors, two of which sit on the newly formed ring.

The most positive region of the molecule, at +45.3 kcal mol^{-1}, is the phenolic hydrogen, the only strong hydrogen-bond donor present. The methoxy oxygen carries a much weaker negative potential, because part of its lone-pair density is donated into the aromatic ring rather than being available at the surface, and the ring oxygen O1 of the lactone is similarly shielded. Read together with the frontier-orbital picture, the map suggests that in a protein binding site the molecule would anchor through the three carbonyls and the phenolic OH, with the three aryl rings providing hydrophobic contact; this is how docking results for related oxazepine and benzoxazepine systems are usually rationalised [10, 17, 37]. The surface pattern is also consistent with the phenolic Schiff base and vanillinoid systems analysed as hydrogen-atom-transfer-active radical scavengers [21, 27].

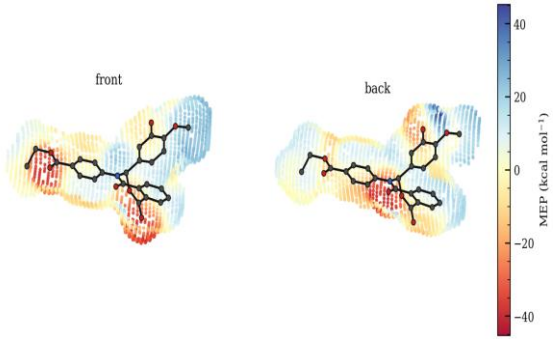

Figure 12: Molecular electrostatic potential mapped on the ρ = 0.001 a.u. electron-density isosurface, front and back views. Red marks the most negative and blue the most positive regions.

3.8. Mulliken and Löwdin population analysis

Mulliken and Löwdin charges are compared in Fig. 13 and the extreme values are given in Table 6 (values are sorted by the Mulliken magnitude). Both schemes agree on the chemistry even though the absolute numbers differ, which is the usual situation. The phenolic oxygen O7 carries the largest negative charge in both partitioning schemes (-0.638 e by Mulliken, -0.440 e by Löwdin) and is the most negative atom overall on both

scales. The methoxy oxygen O6 follows on the Mulliken scale (-0.519 e), whereas on the Löwdin scale the three carbonyl oxygens O3, O4 and O5 (-0.459, -0.455 and -0.412 e) rank above it, a difference that reflects the well-known tendency of the Mulliken scheme to over-weight the diffuse lone pairs of ether oxygens.

On the positive side the three carbonyl carbons stand out, and their ordering is chemically meaningful. The ester carbonyl carbon C1 is the most positive (+0.530 e Mulliken, +0.479 e Löwdin), the lactone carbonyl carbon C12 follows at +0.486 / +0.476 e, and the lactam carbonyl carbon C9 is the least positive of the three at +0.450 / +0.373 e. That ordering is precisely what amide resonance predicts: the nitrogen lone pair pushes electron density onto the lactam carbon and partially neutralises it, whereas the ring oxygen of the lactone is a much poorer donor. The same effect appears at the nitrogen itself, whose Löwdin charge of -0.131 e is remarkably small in magnitude for an amide nitrogen and confirms that the lone pair is concentrated on the carbonyl oxygen rather than on the nitrogen.

The sp^3 N,O-acetal carbon C8 carries only a modest positive charge (+0.134 e Mulliken, +0.182 e Löwdin) despite being flanked by two electronegative heteroatoms, because the two withdrawing effects are partly compensated by donation from the attached aryl ring. One further value needs comment. The terminal methyl carbon C25 appears strongly negative in the Mulliken analysis, at -0.466 e, which is a known partitioning artefact: Mulliken analysis assigns the C–H bonding density to carbon and drives the hydrogens positive, and the effect is largest for a carbon carrying three hydrogens. The Löwdin values are smaller in magnitude and less basis-set dependent, but still show the same trend at C25 (-0.308 e); the ordering among the heteroatoms is preserved, and we quote both schemes for transparency.

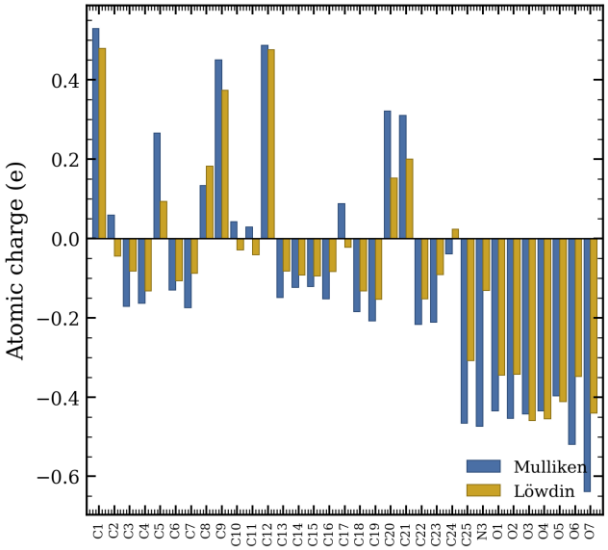

Figure 13: Mulliken and Löwdin atomic charges of the heavy atoms of compound 2.

Table 06: Atoms carrying the largest negative and positive charges. Labels follow Fig. 6; O1 is the ring (lactone) oxygen, O2 and O3 the ester oxygens, O4 the lactam oxygen, O5 the lactone carbonyl oxygen, O6 the methoxy oxygen and O7 the phenolic oxygen.

Atom	Mulliken (e)	Löwdin (e)	Atom	Mulliken (e)	Löwdin (e)
O7	-0.6379	-0.4403	C1	0.5297	0.4788
O6	-0.5191	-0.3486	C12	0.4864	0.4759
N3	-0.4743	-0.1313	C9	0.4501	0.3734
C25	-0.4658	-0.3083	C20	0.3208	0.1517
O2	-0.4534	-0.3424	C21	0.3104	0.1997
O3	-0.4429	-0.4589	C5	0.2661	0.0936

3.9. Thermochemical parameters

Thermochemical quantities from the harmonic analysis at 298.15 K and 1 atm are listed in Table 7. The zero-point vibrational energy is 253.77 kcal mol^{-1} (1061.8 kJ mol^{-1}), a large number simply because the molecule has 54 atoms and 156 vibrational degrees of freedom. The thermal correction to the enthalpy is 1142.66 kJ mol^{-1} and the correction to the Gibbs energy 887.39 kJ mol^{-1}. The total standard entropy of 856.17 J mol^{-1} K^{-1} splits into 207.8 for translation, 155.0 for rotation and 493.4 for vibration, so more than half of it comes from the low-frequency torsional modes of the ethyl, methoxy and aryl groups and from the ring-puckering motion of the seven-membered ring itself; the lowest calculated mode lies at 13.9 cm^{-1}. The rotational constants, 0.059, 0.064, 0.260 GHz, confirm an elongated near-prolate rotor. All 156 modes are real, which establishes that the structure discussed throughout this work is a genuine minimum on the GFN2-xTB potential-energy surface and not a saddle point. These values serve mainly as reference data for later work; the low-frequency modes in particular mean that the harmonic entropy should be treated as an upper bound, since a quasi-harmonic treatment would damp the contribution of modes below about 100 cm^{-1}.

Table 07: Thermochemical data at 298.15 K and 1 atm from the rigid-rotor / harmonic-oscillator model (GFN2-xTB Hessian).

Quantity	Value
Zero-point vibrational energy	253.77 kcal mol^{-1} (1061.8 kJ mol^{-1})
Thermal correction to enthalpy	1142.66 kJ mol^{-1}
Thermal correction to Gibbs energy	887.39 kJ mol^{-1}

Quantity	Value
Total standard entropy	856.17 J mol^{-1} K^{-1}
Translational / rotational / vibrational entropy	207.8 / 155.0 / 493.4 J mol^{-1} K^{-1}
Rotational constants	0.059 / 0.064 / 0.260 GHz
Lowest vibrational wavenumber	13.9 cm^{-1}
Highest vibrational wavenumber	3478.5 cm^{-1}
Number of normal modes	156
Number of imaginary frequencies	0

3.10. Reactive sites and outlook

Putting the pieces together yields a coherent picture, with one reservation that is stated explicitly below. The infrared data establish that the azomethine of 1 has been consumed and that two new, chemically distinct carbonyl groups have been created, and the ^{13}C spectrum shows the same thing at 174.92 and 169.20 ppm alongside the untouched ester at 166.37 ppm. That pattern is what the [2+5] cycloaddition of phthalic anhydride onto an imine is expected to produce and cannot be accounted for by unreacted starting material. The calculations then describe a molecule that is kinetically stable, moderately soft, strongly polar, and organised as a guaiacyl donor and a phthaloyl acceptor joined through an sp^3 carbon that blocks conjugation between them.

Three sites stand out. The phenolic OH is the strongest hydrogen-bond donor, carries the most positive electrostatic potential of the whole surface at +45.3 kcal mol^{-1}, and sits on the fragment that alone constitutes 92% of the HOMO; it is therefore the most likely position for hydrogen-atom transfer, the mechanism by which phenolic antioxidants normally operate [19, 22, 27], so a DPPH assay would be a sensible next experiment, particularly since oxazepines carrying free phenolic groups have already shown measurable radical-scavenging activity [15, 16]. The three carbonyl oxygens are the best acceptors and the most likely coordination sites toward a metal ion, which makes the compound a candidate ligand as well as a drug-like molecule. The three carbonyl carbons are the most electrophilic centres, with the ester and lactone carbons ahead of the lactam carbon, and are where hydrolytic degradation would begin; the lactone of the seven-membered ring is the obvious weak point, and ring-opening hydrolysis towards a phthalamic acid derivative should be expected in strongly aqueous base. The reservation concerns the N,O-acetal carbon. As set out in Section 3.3, no ^{13}C resonance is observed in the 65–110 ppm region where that carbon is expected, and the ^{1}H spectrum of 2 was not available for this study. The infrared evidence, the two new carbonyl resonances and the mass balance all point to the seven-membered ring, but a direct observation of the C-8 methine and of its attached proton is still missing. DEPT-135 and HSQC experiments, a ^{13}C spectrum accumulated with a substantially larger number of transients, and a ^{1}H spectrum of the purified product would settle the point; high-resolution mass spectrometry and CHN analysis, for which the calculated values are given in Section 2.3, would independently confirm the 1:1 composition. These measurements are recommended before the structure is regarded as fully established.

It is also worth being explicit about what the calculations do not cover. Everything reported here refers to a single molecule in the gas phase, whereas the infrared and NMR data were recorded on a solid and in DMSO solution, respectively. The geometry, the frequencies and the thermochemistry are semi-empirical, obtained at the GFN2-xTB level, and only the electronic structure is density-functional; a vibrationally verified B3LYP/6-31G(d) minimum would be the natural next step. Explicit continuum-solvation single-point calculations on structurally related push–pull systems typically shift the individual HOMO and LUMO by 0.01–0.3 eV each and often in the same direction, so that the fundamental gap changes by less than about 0.05 eV. Packing forces in the solid can additionally alter the torsion angles of the flexible substituents, and the twist-boat ring is expected to invert readily in solution, which is itself a plausible cause of the missing C-8 resonance. The C-8 centre is stereogenic; because neither reagent is chiral, the product is a racemate. The two enantiomers are isoenergetic, so every scalar property reported here is identical for both, although an interaction with a chiral biological target would not be.

4. CONCLUSION

Ethyl 4-[2-(3-hydroxy-4-methoxyphenyl)-4,9-dioxo-2,3,4,9-tetrahydro-1,3-benzoxazepin-3-yl]benzoate was prepared in two steps from isovanillin and benzocaine, with phthalic anhydride used to close the seven-membered oxygen–nitrogen ring in a [2+5] cycloaddition that proceeds without loss of a small molecule. The spectroscopic evidence for ring formation rests on three independent infrared markers-loss of the 1642 cm^{-1} azomethine band, appearance of a lactone carbonyl band at 1709 cm^{-1} and appearance of a distinct lactam carbonyl band at 1674 cm^{-1} — supported by a 200 cm^{-1} drop of the phenolic O–H stretch that signals a much stronger hydrogen-bonded network, and on the appearance in the ^{13}C spectrum of two new carbonyl resonances at 174.92 and 169.20 ppm next to the unchanged ester signal at 166.37 ppm. The N,O-acetal carbon of the new ring was not observed and its direct detection by DEPT-135 and HSQC remains outstanding.

The computational study reported here, at the B3LYP/6-31G(d)//GFN2-xTB level, established a twist-boat heterocycle with a Cremer–Pople amplitude of 0.892 Å and the puckering concentrated at the sp^3 carbon, which lies 0.558 Å out of the mean ring plane, with all 156 vibrational modes real and no imaginary

frequency; the calculated harmonic wavenumbers reproduce the measured positions with a mean absolute deviation of 17 cm^{-1} over twenty-four fingerprint bands. The frontier orbitals are cleanly separated in space, the HOMO 92% on the hydroxy/methoxy-substituted ring and the LUMO 51% on the fused benzo ring and 32% on the two new carbonyls, leaving a gap of 4.331 eV. The molecule is a soft one, with a chemical hardness of 2.166 eV and a dipole moment of 7.574 D, and is classified as a strong electrophile (ω = 3.241 eV) and a strong nucleophile (N = 3.205 eV) on the Domingo scale calibrated at the same level of theory, and shows electrostatic-potential values between −38.0 and +45.3 kcal mol^{-1}, with the minimum over the lactone oxygen and the maximum on the phenolic hydrogen. Those positions-the phenolic OH as the hydrogen-atom-transfer donor, the three carbonyl oxygens as electrophile and metal binding sites, and the three carbonyl carbons as sites of hydrolytic degradation-are the ones to watch in any subsequent antioxidant, antimicrobial or coordination study.

5. ACKNOWLEDGEMENTS

The author thanks the General Directorate of Al-Qadisiyah Education, Ministry of Education, for its support, and the staff of the laboratories in which the infrared and NMR spectra of the compounds reported here were recorded. The computational part of this work was carried out entirely with open-source software (PySCF, RDKit and the tblite implementation of GFN2-xTB).

6. AUTHOR CONTRIBUTIONS

Rawaa Naeamah Abdullah: Conceptualisation, Methodology, Investigation, Formal analysis, Validation, Visualisation, Writing – original draft, Writing – review and editing. The author read and approved the final version of the manuscript.

7. FUNDING

This research did not receive any specific grant from funding agencies in the public, commercial, or not-for-profit sectors.

8. CONFLICTS OF INTEREST

The authors declare no competing financial interest.

9. DATA AVAILABILITY

The optimised Cartesian coordinates, the calculated harmonic wavenumbers and infrared intensities, and the scripts used to generate them are available from the corresponding author on reasonable request.

10. REFERENCES

1. H. Farhid, M. Mahyari, A. Abdolmaleki, Y. Mohammadi, Multicomponent reactions for the synthesis of oxazepines, Topics in Current Chemistry, 2026, 384(3), 23. DOI: 10.1007/s41061-026-00551-1.
2. N. Amri, A. A. Abu-Hashem, Design, synthesis, antimicrobial activity and molecular docking of new 1,2,4-triazepine, 1,3,4,6-oxatriazepine and pyridazino[1,2-a]pyrimidine derivatives, Pharmaceuticals, 2026, 19(1), 83. DOI: 10.3390/ph19010083.
3. D. S. Zinad, A. Mahal, R. K. Mohapatra, A. K. Sarangi, M. R. F. Pratama, Medicinal chemistry of oxazines as promising agents in drug discovery, Chemical Biology & Drug Design, 2020, 95(1), 16–47. DOI: 10.1111/cbdd.13633.
4. M. Luczynski, A. Kudelko, Synthesis and biological activity of 1,3,4-oxadiazoles used in medicine and agriculture, Applied Sciences, 2022, 12(8), 3756. DOI: 10.3390/app12083756.
5. A. A. Dawood, S. R. Mohammed, M. Mahmoud, Synthesis, identification and biological activity of new heterocyclic compounds from reaction of new Schiff bases with phthalic anhydride, Science Journal of University of Zakho, 2020, 8(1), 12–18. DOI: 10.25271/sjuoz.2020.8.1.641.
6. O. A. Nief, H. N. Salman, L. S. Ahamed, Synthesis, characterization, biological activity studies of Schiff bases and 1,3-oxazepine derived from 1,1-bis(4-aminophenyl)-4-phenylcyclohexane, Iraqi Journal of Science, 2017, 58(4B), 1998–2011. DOI: 10.24996/ijs.2017.58.4b.2.
7. K. M. Mohammad, M. R. Ahmed, M. H. Mahmoud, Synthesis and characterization of some new (1,3-oxazepine) derivative from 6-methyl-2-thiouracil and study their biological activity, Tikrit Journal of Pure Science, 2017, 22(2), 67–81. DOI: 10.25130/tjps.v22i2.630.
8. R. B. Nadr, B. S. Abdulrahman, Synthesis and characterization of a new series of [1,3]-oxazepine compounds from heterocyclic Schiff bases, Zanco Journal of Pure and Applied Sciences, 2023, 35(2), art. 21. DOI: 10.21271/zjpas.35.2.21.
9. A. J. Mahrath, S. A. Aowda, S. N. Kamil, Synthesis and spectroscopic studies of some new oxazepine derivatives throughout [2+5] cycloaddition reactions (III), Research on Chemical Intermediates, 2013, 39(8), 3739–3752. DOI: 10.1007/s11164-012-0877-2.
10. B. M. Salih, S. R. Mohammed, M. K. Ali, Synthesis development, spectroscopy characterizations, and molecular docking study of some new bis-1,3-oxazepine and bis-1,3-benzoxazepine derivatives, Oriental Journal of Chemistry, 2025, 41(2), 563–572. DOI: 10.13005/ojc/410227.
11. A. H. Kshash, Synthesis and characterization of tetrachloro-1,3-oxazepine derivatives and evaluation of their biological activities, Acta Chimica Slovenica, 2020, 67(1), 113–118. DOI: 10.17344/acsi.2019.5264.
12. A. K. N. Allamy, S. A. Mejbel, Preparation, characterization and biological activity of some new seven-membered heterocyclic compounds, World Journal of Advanced Research and Reviews,

2022, 15(1), 662–678. DOI: 10.30574/wjarr.2022.15.1.0744.
13. S. J. Khan, S. S. Marufa, M. I. Sultan, A. T. Aurora, J. R. Debnath, S. Easmin, H. Nishino, M. A. Haque, M. M. Rahman, Novel thiophene–thiazole-Schiff base hybrids: design, synthesis, antimicrobial and antioxidant activity with ADMET prediction, molecular docking and dynamics study, RSC Advances, 2025, 15(53), 45690–45706. DOI: 10.1039/D5RA07357J.
14. D. Kumar, N. Aggarwal, H. Kumar, G. Kapoor, A. Deep, S. Bibi, A. Sharma, H. Chopra, R. K. Marwaha, A. Alshammari, M. Alharbi, A. Hayee, 2-Substituted-3-(5-substituted-1,3,4-oxadiazol/thiadiazol-2-yl)thiazolidin-4-one derivatives: synthesis, anticancer, antimicrobial, and antioxidant potential, Pharmaceuticals, 2023, 16(6), 805. DOI: 10.3390/ph16060805.
15. S. K. Singh, N. Mishra, G. Nayak, P. Mehta, Synthesis of Schiff base derivatives of 1,3-oxazepine and evaluation of antioxidant action in vitro, Oriental Journal of Chemistry, 2023, 39(5), 1367–1372. DOI: 10.13005/ojc/390534.
16. A. G. Sager, J. K. Abaies, Z. R. Katoof, Molecular docking, synthesis and evaluation for antioxidant and antibacterial activity of new oxazepane and benzoxazepine derivatives, Baghdad Science Journal, 2024, 21(7), 2289. DOI: 10.21123/bsj.2023.8553.
17. S. A. Hassan, D. M. Aziz, M. N. Abdullah, A. R. Bhat, R. S. Dongre, S. Ahmed, A. K. Rahiman, T. B. Hadda, M. Berredjem, J. Jamalis, Design and synthesis of oxazepine derivatives from sulfonamide Schiff bases as antimicrobial and antioxidant agents with low cytotoxicity and hemolytic prospective, Journal of Molecular Structure, 2023, 1292, 136121. DOI: 10.1016/j.molstruc.2023.136121.
18. R. S. Kumar, S. Naveena, S. Praveen, N. Yogadharshini, Therapeutic aspects of biologically potent vanillin derivatives: a critical review, Journal of Drug Delivery and Therapeutics, 2023, 13(7), 177–189. DOI: 10.22270/jddt.v13i7.6159.
19. B. Demirbağ, M. Yildirim, M. Cimentepe, A. Necip, H. Unver, E. N. Tiftik, Novel vanillin-derived Schiff bases: synthesis, characterization, antibacterial activity, enzyme inhibition, antioxidant activity, anti-inflammatory activity on LPS-induced RAW264.7 macrophage cell line, and in silico studies, Journal of Molecular Structure, 2025, 1338, 142320. DOI: 10.1016/j.molstruc.2025.142320.
20. R. Khan, S. Rashid, S. Khan, Y. A. Almutawif, B. Pari, Synthesis and evaluation of vanillin Schiff bases as potential antimicrobial agents against ESBL-producing bacteria: towards novel interventions in antimicrobial stewardship, Scientific Reports, 2024, 14, 28007. DOI: 10.1038/s41598-024-78302-9.
21. N. Yuldasheva, N. Acikyildiz, M. Akyuz, L. Yabo-Dambagi, T. Aydin, A. Cakir, C. Kazaz, The synthesis of Schiff bases and new secondary amine derivatives of p-vanillin and evaluation of their neuroprotective, antidiabetic, antidepressant and antioxidant potentials, Journal of Molecular Structure, 2022, 1270, 133883. DOI: 10.1016/j.molstruc.2022.133883.
22. R. Karthika, S. Nandhini, S. Suriya, T. Pooventhiran, A. Y. A. Alzahrani, R. Thomas, Synthesis of vanillin derivative Schiff's bases from threonine and valine: structural study and multiscale computational modeling, Biochemical and Biophysical Research Communications, 2025, 781, 152501. DOI: 10.1016/j.bbrc.2025.152501.
23. F. Lemilemu, M. Bitew, T. B. Demissie, R. Eswaramoorthy, M. Endale, Synthesis, antibacterial and antioxidant activities of thiazole-based Schiff base derivatives: a combined experimental and computational study, BMC Chemistry, 2021, 15, 67. DOI: 10.1186/s13065-021-00791-w.
24. N. Elangovan, R. Thomas, S. Sowrirajan, Synthesis of Schiff base (E)-4-((2-hydroxy-3,5-diiodobenzylidene)amino)-N-(thiazol-2-yl)benzenesulfonamide with antimicrobial potential, structural features, experimental biological screening and quantum mechanical studies, Journal of Molecular Structure, 2022, 1250, 131762. DOI: 10.1016/j.molstruc.2021.131762.
25. O. E. Oyeneyin, N. D. Ojo, N. Ipinloju, E. B. Agbaffa, A. V. Emmanuel, Investigation of the corrosion inhibition potentials of some 2-(4-(substituted)arylidene)-1H-indene-1,3-dione derivatives: density functional theory and molecular dynamics simulation, Beni-Suef University Journal of Basic and Applied Sciences, 2022, 11, 132. DOI: 10.1186/s43088-022-00313-0.
26. G. Ramesh, B. Venkatram Reddy, Investigation of barrier potential, structure (monomer and dimer), chemical reactivity, NLO, MEP, and NPA analysis of pyrrole-2-carboxaldehyde using quantum chemical calculations, Polycyclic Aromatic Compounds, 2023, 43(5), 4216–4230. DOI: 10.1080/10406638.2022.2086889.
27. M. Molski, Theoretical study on the radical scavenging activity of gallic acid, Heliyon, 2023, 9(3), e12806. DOI: 10.1016/j.heliyon.2023.e12806.
28. A. A. Hassan, S. Bräse, A. A. Aly, H. N. Tawfeek, Chemistry of substituted thiazinanes and their derivatives, Molecules, 2020, 25(23), 5610. DOI: 10.3390/molecules25235610.
29. Q. Sun, X. Zhang, S. Banerjee, P. Bao, M. Barbry, N. S. Blunt et al., Recent developments in the PySCF program package, Journal of Chemical Physics, 2020, 153(2), 024109. DOI: 10.1063/5.0006074.
30. C. Bannwarth, S. Ehlert, S. Grimme, GFN2-xTB — an accurate and broadly parametrized self-consistent tight-binding quantum chemical method with multipole electrostatics and density-dependent dispersion contributions, Journal of

Chemical Theory and Computation, 2019, 15(3), 1652–1671. DOI: 10.1021/acs.jctc.8b01176.
31. L. R. Domingo, M. Ríos-Gutiérrez, P. Pérez, Applications of the conceptual density functional theory indices to organic chemistry reactivity, Molecules, 2016, 21(6), 748. DOI: 10.3390/molecules21060748.
32. M. Ríos-Gutiérrez, A. Saz Sousa, L. R. Domingo, Electrophilicity and nucleophilicity scales at different DFT computational levels, Journal of Physical Organic Chemistry, 2023, 36(7), e4503. DOI: 10.1002/poc.4503.
33. D. Cremer, J. A. Pople, General definition of ring puckering coordinates, Journal of the American Chemical Society, 1975, 97(6), 1354–1358. DOI: 10.1021/ja00839a011.
34. [34] D. Majumdar, A. Chatterjee, M. Feizi-Dehnayebi, N. S. Kiran, B. Tuzun, D. Mishra, 8-Aminoquinoline derived two Schiff base platforms: synthesis, characterization, DFT insights, corrosion inhibitor, molecular docking, and pH-dependent antibacterial study, Heliyon, 2024, 10(15), e35591. DOI: 10.1016/j.heliyon.2024.e35591.
35. M. Khalid, A. Ali, M. F. Ur Rehman, M. Mustaqeem, S. Ali, M. U. Khan, S. Asim, N. Ahmad, M. Saleem, Exploration of noncovalent interactions, chemical reactivity, and nonlinear optical properties of piperidone derivatives: a concise theoretical approach, ACS Omega, 2020, 5(22), 13236–13249. DOI: 10.1021/acsomega.0c01273.
36. M. Khadka, M. Sah, R. Chaudhary, S. K. Sahani, K. Sahani, B. K. Pandey, D. Pandey, Spectroscopic, quantum chemical, and topological calculations of the phenylephrine molecule using density functional theory, Scientific Reports, 2025, 15, 208. DOI: 10.1038/s41598-024-81633-2.
37. M. El-Naggar, H. R. M. Rashdan, A. H. Abdelmonsef, Cyclization of chalcone derivatives: design, synthesis, in silico docking study, and biological evaluation of new quinazolin-2,4-diones incorporating five-, six-, and seven-membered ring moieties as potent antibacterial inhibitors, ACS Omega, 2023, 8(30), 27216–27230. DOI: 10.1021/acsomega.3c02478.